Front. Chem. Sci. Eng. 2020, 14(4): 579–594
https://doi.org/10.1007/s11705-018-1770-3

RESEARCH ARTICLE

Parametric study on the mixed solvent synthesis of ZIF-8 nano- and micro-particles for CO adsorption: A response surface study

Alireza Hadi[1], Javad Karimi-Sabet (✉)[2], Abolfazl Dastbaz[1]

1 Department of Chemical Engineering, Faculty of Engineering, University of Tehran, Tehran, Iran
2 Material and Nuclear Fuel Research School (MNFRS), Nuclear Science and Technology Research Institute, Tehran, Iran

Abstract The room temperature synthesis of ZIF-8 micro- and nano-particles was investigated using a mixed methanol-water solvent system. ZIF-8 particles of good quality and high crystallinity were obtained. Response surface methodology was used to determine the effect of the synthesis conditions on the ZIF-8 yield, particle size distribution, and mean particle size. The ligand/metal salt molar ratio followed by the amount of sodium formate (the deprotonating agent) and then the amount of water (i.e., the composition of the mixed solvent) respectively had the largest effects on both the ZIF-8 yield and particle size. Results showed that mixing of solvents with different strengths in producing ZIF-8 crystals is a practical method to size-controlled synthesis of ZIF-8 particles. This method is more favorable for industrial-scale ZIF-8 synthesis than using excess amounts of ligands or chemical additives (like sodium formate). In addition, ZIF-8 samples with different mean particle sizes (100, 500, and 1000 nm) were used for CO adsorption and the mid-sized ZIF-8 particles had the highest adsorption capacity.

Keywords metal organic frameworks, zeolitic imidazolate frameworks, ZIF-8, response surface methodology, Box Behnken design, CO adsorption

1 Introduction

Nowadays, the organic-inorganic 3D structures so-called metal organic frameworks (MOFs) gained have great importance as a unique type of the porous materials. As the name implies, MOFs are constructed from repeating molecular scaffolds in which metal atoms or clusters act as nodes and are connected by organic ligands which serve as rigid bridges [1]. Due to the variety of building elements that can be used, many different molecular designs can be made and this has resulted in the variety of MOFs with more types continuously being developed [2]. MOFs typically have 3D network-like structures and many excellent properties including high porosities (up to 90%), extremely high surface areas (up to 6000 m^2/g), molecular-sized pores with narrow distributions, designable pore sizes and shapes, and ease of functionalization by organic components [3]. Another great feature of MOFs is their ability to incorporate molecules into their structures via various host-guest interactions which endows the MOFs with new properties [4]. In addition to what has been mentioned above, some MOFs have attractive properties that are exclusively related to specific groups contained within those MOFs. For example magnetic MOFs [5], have magnetic metal nodes or clusters (such as Fe and Co) in their structures giving them magnetic properties [6–8]. These many diverse special properties have resulted in a wide variety of applications for MOFs in areas such as gas storage [9–11], gas separation [12–16], heterogeneous catalysis [17–19], drug delivery [20,21], capture and degradation of toxic gases [22], sensors [23–25], and energy storage (batteries and supercapacitors) [26,27].

Zeolitic imidazolate frameworks (ZIFs) are a well-known category of MOFs that have been extensively studied since their introduction by Yaghi's group in 2006 [28]. ZIFs have a zeolite-like structure in which the metal ions or clusters, and the organic ligands are in the same configuration as silicon and oxygen in zeolites. The bond angles between the tetrahedral metal ions (Zn, Co) and the ligands (imidazolate) are approximately 145°, which is similar to the M-O-M bonds in zeolites (M = Si and/or Al, O = oxygen). Their high thermal and chemical stabilities make ZIFs different from other MOFs since most MOFs

Received April 18, 2018; accepted August 19, 2018

E-mails: j_karimi@alum.sharif.edu, jvkarimi@aeoi.org.ir

suffer from low thermal and chemical stabilities and in fact this has hindered the development of various applications for MOFs. The most widely studied and used ZIFs is ZIF-8. This MOF has a sodalite topology with pore sizes of 11.6 Å, pore apertures of 3.4 Å, a surface area of 1947 m^2/g and a pore volume of 0.663 cm^3/g [28]. Owing to its excellent features, ease of preparation, and its wide applications, ZIF-8 is produced commercially. There are several different methods to prepare ZIFs including room temperature synthesis [29] hydrothermal [30], solvothermal [31], sonochemical [32], mechanochemical [33], electrochemical [34], dry-gel conversion [35], microfluidic [36], and microwave assisted [37] methods. Among these methods, room temperature synthesis has the benefits of being simple since no special or complex experimental setup is needed and very fast. In addition, this method has low energy consumption compared to other common routes like solvothermal and sonochemical methods. Therefore, room temperature crystallization is a powerful technique for preparing nano-sized ZIFs even on a large scale.

Due to the important effect of particle size on the properties and applications of nanoparticles [38–41], efficient synthesis methods that provide control over particle size are usually desirable. ZIF-8 is no exception and there have been some studies on tuning ZIF-8 particle sizes. For example, different additives such as triethylamine [42], *n*-butylamine, sodium formate, 1-methylimidazole [43], and NaOH [44] have been introduced to ZIF-8 synthesis mixtures as deprotonating and modulating agents to improve the yield or manipulate the final crystal size by controlling the crystallization process. Polyzoidis et al. used microreaction technology for the high-yield, large-scale production of ZIF-8 with tunable particle sizes [45]. Other studies have focused on the type of zinc precursor. For example, Jian et al. studied the effect of six different zinc precursors on the quality and morphology of ZIF-8 synthesized at room temperature and concluded that Zn $(OAc)_2$, which gave ZIF-8 particles with a rhombic dodecahedron morphology, was the best [46]. In other research, Chi et al. used zinc nitrate, zinc acetate and zinc chloride as precursors and produced particle sizes of 88, 240 and 533 nm, respectively [47].

Herein, solvent composition has been varied in order to manipulate ZIF-8 particle size. Due to environmental concerns, replacing organic solvents with water as a cheap, nontoxic, and nonflammable solvent is always desirable in any chemical processes. In this regard, the present study investigates the synthesis of ZIF-8 particles in a mixed solvent (methanol-water) at room temperature. The effect of different preparation factors on the ZIF-8 synthesis yield, particle size distribution and mean particle size were investigated via response surface methodology. The factors examined include the ligand content, the amount of sodium formate additive, and the composition of the methanol-water solvent. The ZIF-8 particles were characterized by different methods to investigate their crystallinity, pore sizes, surface areas, and particle sizes. Finally, the effect of the ZIF-8 particle size on CO adsorption was also determined.

2 Experimental

2.1 Materials

Zinc nitrate hexahydrate was obtained from Sigma Aldrich. All other chemical reagents including methanol, 2-methylimidazole (2-MeIM) and sodium formate were purchased from Merck Co. and were used directly without any purification. Carbon monoxide (99.99%) gas was provided from Farafan Gas Co. and used as received. Double distilled water was used in any experiments using water as the co-solvent.

2.2 Methods

2.2.1 Room temperature synthesis of ZIF-8

The synthesis procedure for ZIF-8 was based on the method reported by Cravillon et al. [48] and the modified recipe reported by Zhang et al. [49]. In a typical experiment, the desired amount of zinc nitrate was dissolved in 25 mL of solvent. Then a second solution was prepared by dissolving the desired amounts of 2-methylimidazolate and sodium formate in 25 mL of solvent. In the case of mixed-solvent syntheses, water and methanol were mixed in the desired ratios to obtain 50 mL of mixed solvent and this was then divided into two 25-mL portions and used as stated above. After the two solutions were prepared the ligand solution was rapidly poured into the zinc solution with mild stirring (At higher concentrations of 2-MeIM, the mixture immediately became opaque after blending). The solution was continuously stirred at room temperature during the course of the reaction. After 24 h, the stirring was stopped and the mixture was centrifuged at 5000 r/min for 10 min. The solid product was washed repeatedly with fresh methanol and acetone and then the products were dried at 50°C overnight before being subjected to further analysis.

2.2.2 Characterization

X-ray diffraction (XRD) was carried out using a X'Pert PRO MPD diffractometer (PANalytical Company) with Cu Kα radiation (λ = 1.5406 Å) that was operated at 40 kV and 40 mA. Scanning was conducted between 2θ values of 5° and 40° with a step size of 0.026°. The morphology and particle sizes of the synthesized ZIF-8 were determined by field emission scanning electron microscopy (FE-SEM). A small amount of the final solution was decanted and used as the FESEM sample. FESEM images were captured

using a TESCAN MIRA3 field emission scanning electron microscope. Particle size distributions were obtained by statistical evaluation of about 100 particles using Image J 1.47V (NIH, USA) software. The mean particle size was determined by Gaussian fitting of the resultant particle size distribution. The N_2 adsorption-desorption isotherm of the ZIF-8 powder was obtained at 77 K using a Belsorp mini II (Bel company, Japan) volumetric adsorption measurement instrument. Thermogravimetric analysis (TGA) was performed using a Rheometric scientific STA 1500, in the temperature range of 20°C to 700°C at a rate of 10°C/min. Optical absorbance measurements of the ZIF-8 dispersions were obtained with an UV–vis spectrometer (Mecasys, OPTIZEN POP, Korea).

2.2.3 Adsorption of carbon monoxide

Carbon monoxide static adsorption tests were conducted using a volumetric experimental set-up which is shown schematically in Fig. 1. First, the samples were degassed by treating them with nitrogen at 160°C for 4 h. Then, the samples were kept under vacuum at 85°C for another 4 h in order to activate the ZIF-8 particles. For adsorption tests, about 1.5 g of ZIF-8 powder was placed in the gas adsorption cell. Afterward, the adsorption experiments were conducted by injecting enough CO gas to reach pressures between 0 and 10 bar. The temperature was held constant at 25°C. The temperatures of both the loading and adsorption cells were precisely controlled using a water bath. The pressure in the adsorption cell was measured with a pressure transducer (ECO-1, WIKA) with an accuracy of 1%. The system was maintained at each operational pressure for 30 min to establish steady-state conditions. The adsorption tests were repeated three times and the average value is reported.

2.2.4 Response surface methodology (Box-Behnken design)

Response surface methodology (RSM) is an accurate technique for the systematic investigation and optimization of different processes in which the effects of individual variables on a process are unknown [50]. In addition, interactions between factors can be obtained using RSM. In this method, mathematical and statistical calculations are performed based on an experimental design which leads to process optimization. In this work, Box-Behnken which is a well-known incomplete 3^k factorial design was used to investigate the synthesis process of ZIF-8. Design Expert software (version 10.0.1.0, Stat-Ease Inc., Minneapolis, MN, USA) was used for the design and analysis of the experiments, and to plot the results. The amounts of 2-MeIM and sodium formate and the composition of the solvent (methanol-water mixture) were chosen as the main factors. According to the Box- Behnken design, these factors should be studied at three levels so the actual values of these independent factors were coded to $(-1, 0, +1)$ levels according to the equation:

$$x_i = \frac{X_i - X_0}{\Delta X}, \tag{1}$$

where x_i is the coded value of each independent factor, ΔX is the step change value, and X_i, X_0 are the actual and central values of the independent factors, respectively. Table 1 shows the coded and actual values of the selected parameters.

The relationship between the independent factors and the responses can be expressed by a polynomial equation such as linear, quadratic, and cubic models. In this study, a general cubic model represented by the following equation was used:

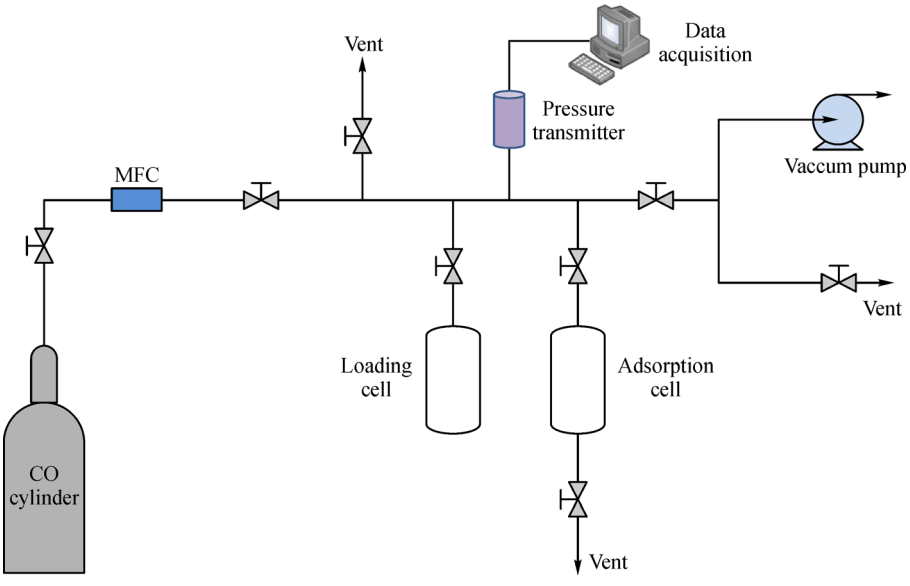

Fig. 1 Schematic diagram of the experimental apparatus for CO static adsorption

Table 1 Coded and un-coded values of factors used in Box-Behnken design

Coded values	2-MeIM molar ratio (A)	Sodium formate molar ratio (B)	Water /vol-% (C)
−1	2	0	0
0	5	2	25
+1	8	4	50

$$Y = \beta_0 + \sum_i^k \beta_i x_i + \sum_i^k \beta_{ii} x_i^2 + \sum_i \sum_j \beta_{ij} x_i x_j + \sum_i^k \beta_{iii} x_i^3 + \sum_i \sum_j \beta_{iij} x_i^2 x_j + \sum_i \sum_j \sum_l \beta_{ijl} x_i x_j x_l, \quad (2)$$

where Y represents the predicted response, x_i, x_j, and x_l denoted the independent variables, k is the number of variables, β_0 is the model constant, β_i is the coefficient for the linear parameters, β_{ii} is the coefficient for the quadratic parameters, β_{ij} is the coefficient for the quadratic crossed parameters, β_{iii} is the coefficient of the cubic single term, β_{iij} is the coefficient of the cubic two cross product terms, and β_{ijl} represents the coefficient of the cubic three cross product terms [51].

The effect of the chosen parameters on two important responses: synthesis yield and mean particle size were explored. Weighing is a common way to calculate MOF synthetic yields, but this only gives an approximate yield because a considerable amount of ZIF-8 particles are lost during the various process steps especially during centrifugation and drying of the products (by adhesion to the experimental vessels). Further, in some experiments, the yield is too low to determine by weighting. Therefore weight is not a very suitable way to calculate yield so a better method was needed. The synthesis yield was determined by UV-vis spectroscopy. The absorbance of ZIF-8 dispersion at 660 nm versus ZIF-8 concentration was measured and shown in Fig. 2. The absorbance is linear ($R^2 = 0.999$) with ZIF-8 concentration and obeys the Beer-Lambert Law. So the concentrations of ZIF-8 were determined by simply measuring the absorbance of the final ZIF-8 dispersions at 660 nm. All samples were diluted to 200 mL before measuring absorbance. Finally, the yield was calculated by dividing the concentration of ZIF-8 by the initial concentration of zinc as a basis. It should be noted that in all experiments 2-MeIM was used in excess.

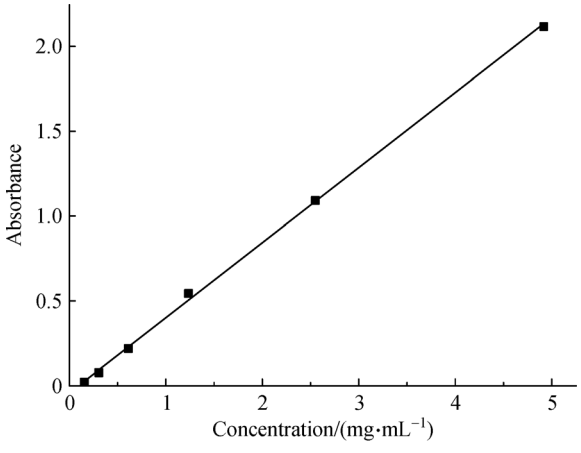

Fig. 2 Absorbance of ZIF-8 in methanol-water dispersion (25% water) at 660 nm versus ZIF-8 concentration

The second response, ZIF-8 particle size, was evaluated using the particle size distribution and the mean particle size which were obtained from the FE-SEM images.

3 Results and discussion

3.1 Characterization

In this study, mixture of methanol and water was used as solvent for room temperature crystallization of ZIF-8 particles. This procedure has not previously been reported for ZIF-8 preparation so XRD was used to investigate the crystallinity and the purity of the samples. Figure 3 shows the XRD pattern of ZIF-8 prepared in pure methanol along with a simulated pattern for a standard ZIF-8 sample [28]. The similarity of these two spectra confirms that highly crystalline pure ZIF-8 particles were obtained in pure methanol.

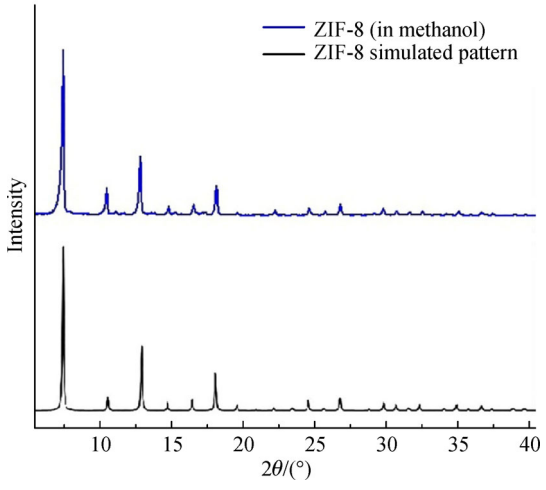

Fig. 3 XRD pattern of ZIF-8 powder synthesized in pure methanol, accompanied by ZIF-8 simulated pattern

When water was added to methanol during the synthesis of ZIF-8, the suspension did not precipitate completely during centrifugation. So in these cases, both the sediments and supernatants were subjected to XRD analysis. The XRD patterns of the products obtained at 1 h in different compositions of methanol-water are shown in Fig. 4. All of these spectra, whether for supernatant or sediment, are quite different from the simulated ZIF-8 pattern. So at 1 h, the sediment and supernatant both probably contain

unreacted components, intermediate crystallization products and/or by-products. These have been previously reported in the synthesis of ZIF-8 in pure water by Nordin et al. [52] and Jian et al. [46]. In order to better probe the effect of water on ZIF-8 crystallization, the reaction was allowed to continue for 24 h.

The XRD patterns of the materials prepared at 24 h are also shown in Fig. 4. Interestingly, these XRD patterns have high correspondence with the ZIF-8 simulated pattern, and prove that the produced particles are pure, crystalline ZIF-8. The spectra of the ZIF-8 powder synthesized at 24 h with different methanol-water mixture (0 to 50% water) are all very similar. The main XRD peaks for all the ZIF-8 samples are at 2θ values of about 7.35°, 10.4°, 12.75°, 14.73°, 16.48° and 18.07° which correspond to (011), (002), (112), (022), (013) and (222) crystal facets, respectively [28]. A closer look at Fig. 4 shows that the 1-h samples contain some of the ZIF-8 standard peaks, specifically there are peaks related to the (002), (112), (013) and (222) crystal facets. The fact that the other peaks disappear at a longer reaction time (24 h) and that only peaks for pure ZIF-8 remain, is good evidence that the 1-h methanol-water products are intermediate products of ZIF-8.

FE-SEM was employed to observe the morphology of the ZIF-8 particles prepared at different conditions and a typical image is shown in Fig. 5. Under all conditions, the most common ZIF-8 morphology was rhombic octahedral, although sometimes other morphologies such as cubic-like and rod-shaped were also observed (Figs. 5(b,c)). These were fairly rare and were most likely to occur under conditions which lead to larger particle sizes. It is noteworthy that both well-defined sharp facets and rounded edge particles were observed in the different samples.

Figure 6 shows the N_2 adsorption-desorption isotherm and the pore size distribution of the ZIF-8 sample synthesized in pure methanol. The Type-1 isotherm is indicative of microporosity in the ZIF-8 particles. The surface area and pore diameter were calculated using the adsorption data with the BET method and the results are given in Table 2. Other information including pore volume, total pore area, and pore diameter which was derived from the BJH method is summarized in Table S1 (cf. Electronic Supplementary Material (ESM)).

Thermal stability is one of the most important characteristics for high-temperature applications of porous materials. So the thermal stability of the prepared ZIF-8 was evaluated by TGA from 20°C to 700°C and the results are shown in Fig. 7. As the sample was heated, it underwent three weight loss stages. The first was a 6% weight loss that occurred at temperatures below 225°C. This loss is related to release of moisture as the guest molecules adsorbed by the ZIF-8 powder [53]. Between 225°C and 400°C there is a plateau region with a slight weight loss of about 5%. This can be attributed to evaporation of the methanol solvent molecules trapped in the ZIF-8 structure during synthesis. The third weight loss occurs between 400 and above 523°C and is about 55%. This loss is related to the thermal decomposition of the ZIF-8 structure. These results show that the prepared ZIF-8 has a good thermal stability up to 400°C which is suitable for many applications.

3.2 ZIF-8 synthesis mechanism

The possible mechanism for the ZIF-8 crystallization is shown in Fig. 8 [54]. The ZIF-8 synthesis at room temperature consists of several stages. First, several different complexes form between the ligands and the Zn^{2+} cations [43]. Next the ligands become deprotonated at which time the 2-methylimidazole loses its pyrimidinic

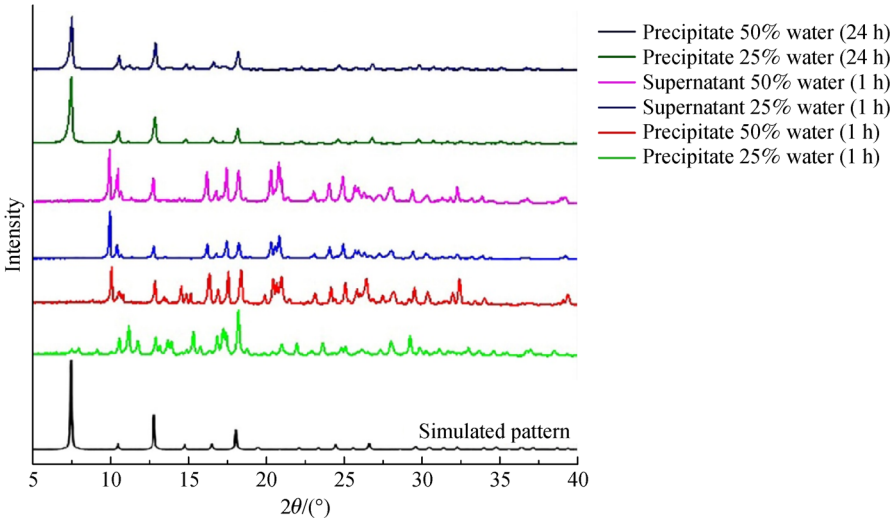

Fig. 4 XRD patterns of materials prepared in methanol-water mixtures containing 25% and 50% vol water at 1 and 24 h reaction times, along with the simulated pattern of ZIF-8

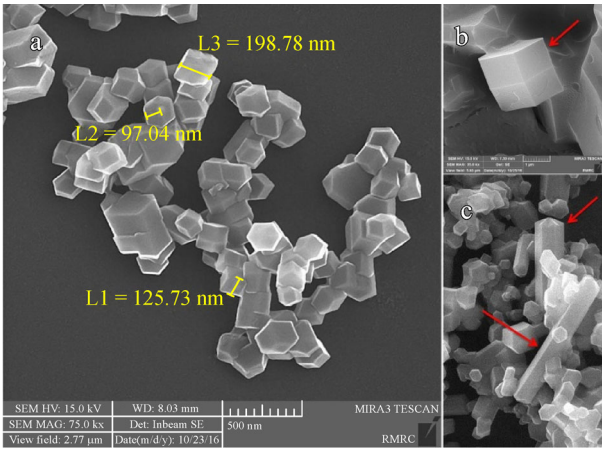

Fig. 5 (a) FE-SEM images showing common rhombic octahedron morphology of ZIF-8 particles (synthesis condition: A = 8, B = 2, C = 0); (b) and (c) FE-SEM images which contain other morphologies rarely observed in ZIF-8 samples (synthesis conditions for (b) A = 2, B = 2, C = 50 and (c) A = 2. B = 4, C = 25)

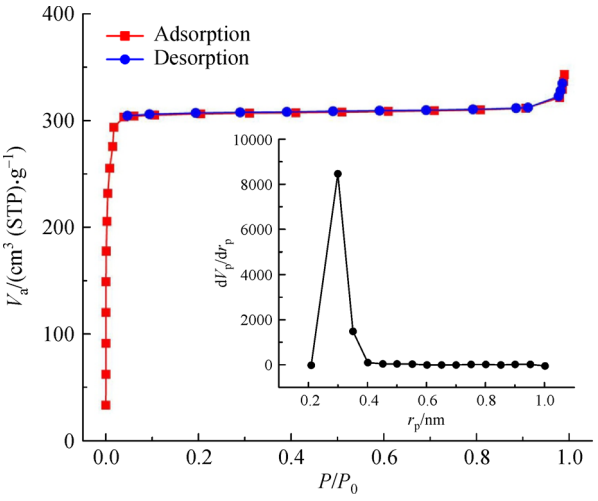

Fig. 6 N_2 adsorption-desorption isotherm of ZIF-8 sample produced in methanol; inset: pore size distribution of ZIF-8 using the BJH method

Table 2 BET parameters and analysis for ZIF-8 synthesized in pure methanol

BET parameters		BET analysis		
c	V_m/(cm^3(STP)·g^{-1})	Surface area $a_{S\ BET}$ /(m^2·g^{-1})	Total pore volume (p/p_0 = 0.99) /(cm^3·g^{-1})	Mean pore diameter/ nm
1798.8	279.5	1216.5	0.5302	1.7434

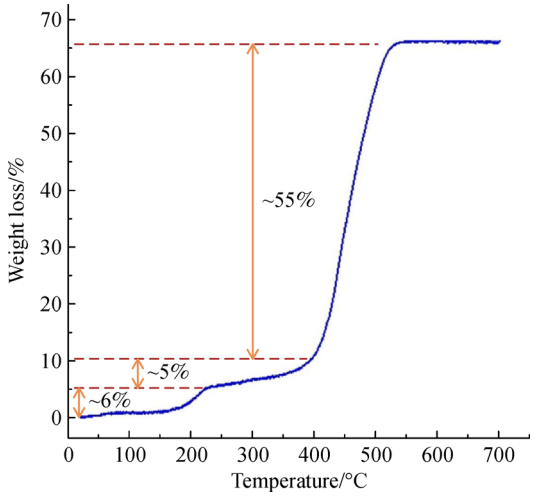

Fig. 7 TGA curve of ZIF-8 synthesized in pure methanol

hydrogen to form an imidazolium anion. The deprotonated ligands then coordinate to the zinc cations to form the primary ZIF-8 building units. This coordination reaction continues and eventually ZnN_4 clusters, which are considered the secondary building units of ZIF-8, are formed. These clusters then form six-membered rings resulting in ZIF-8 nucleation sites (the nucleation step). Other building units then attach to the nuclei causing ZIF-8 crystal growth (the growth step). The nucleation and growth rates both greatly affect the final ZIF-8 particle size and synthesis yield [55,56] and this will be discussed in more detail later.

3.3 RSM model development

A Box Behnken design was used to model the ZIF-8 synthesis process using the selected factors. The experimental conditions and the corresponding responses are tabulated in Table 3. The analysis of variance of the obtained reduced cubic models for ZIF-8 synthesis yield and particle size are presented in Tables S4 and S5, respectively. These results show that both models are statistically significant (p-value < 0.05).

For both models, the backward option of Design-Expert software was used to remove non-significant terms in order to obtain the final reduced models. For the ZIF-8 yield model, the interactive effect between 2-MeIM content and sodium formate content (AB) were insignificant while all other terms were significant (p-value < 0.05). For the ZIF-8 particle size model, the interactions between the 2-MeIM and sodium formate contents (AB), and between the 2-MeIM and water contents (AC) were non-significant (p-value > 0.05). Table 4 shows the final equations of the reduced cubic models for ZIF-8 synthesis yield and mean particle size. The regression coefficients (R^2) and adjusted regression coefficients (R^2_{adj}) for both models are very close

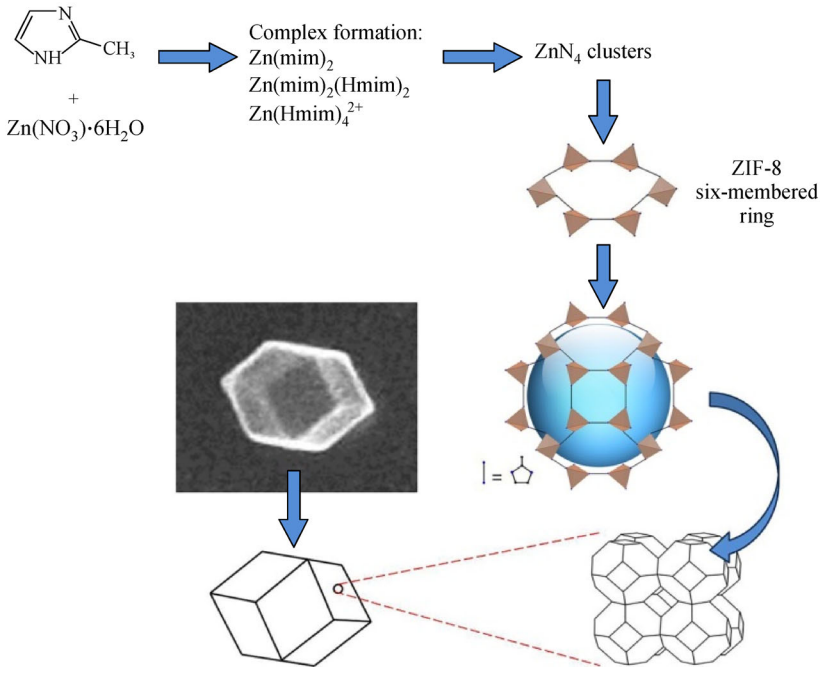

Fig. 8 Simplified diagram of ZIF-8 synthesis mechanism

Table 3 Box- Behnken design matrix and corresponding responses

Experiment No.	Un-coded factors			Responses	
	A: 2-MeIM molar content /x[a)]	B: Sodium formate molar content /y[a)]	C: Water volume percent /vol-%	Yield /wt-%	Particle size /nm
1	8	2	50	7.87	83.4
2	5	2	25	11.31	125.3
3	5	4	50	51.89	185.6
4	5	4	0	48.81	574.8
5	8	2	0	65.54	242.8
6	2	4	25	6.64	687.2
7	8	0	25	11.07	93.98
8	2	2	50	8.11	3876.0
9	5	2	25	12.17	126.3
10	5	0	0	63.56	84.5
11	8	4	25	13.52	116.5
12	5	0	50	48.20	191.3
13	5	2	25	11.68	177.0
14	2	0	25	5.23	706.8
15	2	2	0	1.72	3051.0

a) Zinc nitrate hexahydrate : 2-MeIM : Sodium formate : solvent = 1: x: y: 1000 on molar basis.

or equal to one suggesting that both cubic models properly fit the experimental data.

3.3.1 Effect of factors on ZIF-8 synthesis yield

In order to analyze the impact of synthesis condition on the yield of ZIF-8 production, it is crucial to know how the yield is affected by different parameters. Generally, ZIF-8 particles are synthesized through the nucleation and growth processes. Thus, increasing the nucleation and growth rates by changing the synthesis condition will result in the higher ZIF-8 yield. Inversely, Factors that

Table 4 Reduced cubic models in terms of coded factors for prediction of ZIF-8 yield and mean particle size which obtained using RSM

Response	Reduced model	R^2	R^2_{adj}
ZIF-8 yield	Yield = + 11.72 + 15.89 A − 2.76 B − 3.07 C − 16.02 AC + 4.61 BC − 17.46 A^2 + 14.85 B^2 + 26.55 C^2 + 3.73 A^2B − 9.75 A^2C − 12.71 AB^2	1.000	0.9997
ZIF-8 mean particle size	Particle size = + 142.87 − 1462.55 A + 121.15 B − 70.60 C − 124.0 BC + 1000.08 A^2 − 741.82 B^2 + 858.01 C^2 − 120.42 A^2B + 424.65 A^2C + 1166.67 AB^2	0.9999	0.9993

hinder the reaction and prevent precursors from participating in ZIF-8 nucleation and growth suppress the synthesis yield. In addition, when comparing the absorbance of two different ZIF-8 suspensions at the same ZIF-8 concentration, the suspension with larger particles absorb more UV-vis light which causes an apparent yield seems to be higher. With this in mind, it is possible to discuss the effect of the preparation condition on ZIF-8 yield.

Figure 9 shows the impact of chosen parameters on the yield of ZIF-8. The corresponding 3D RSM plots of the effect of parameters on the yield of ZIF-8 have been shown in Fig. 10. The trends showed in Figs. 9(a,b) are unchanged for the whole studied range as presented in Figs. 10(a,c). But, the impact of 2-MeIM on the yield becomes different by variation of water content (Fig. 10(b)) as discussed below. When the ligand (2-MeIM) molar content was less than 3.4, no ZIF-8 was produced (Fig. 9(a)). The ZIF-8 yield increased to a maximum for a 2-MeIM molar ratio of about 6.3 and larger amounts of 2-MeIM resulted in lower yields. In general, during ZIF-8 synthesis using a pure solvent, a higher amount of 2-MeIM with a constant metal salt content should cause the nucleation to occur more quickly resulting in a higher crystallization rate which in turn leads to higher ZIF-8 yields. But, It is noteworthy to mention that the results presented in Fig. 9 were obtained with the water content at the middle level (25 vol-%). The RSM results (Fig. 10(b)) showed that the descending trend of ZIF-8 yield at high levels of 2-MeIM did not observed when pure methanol was used for the synthesis. The different results for the two solvents systems may be because fewer nuclei are formed in the presence of water than in pure methanol due to the formation of zinc hydroxide, and because there are less free ligands in the water containing mixtures [57].

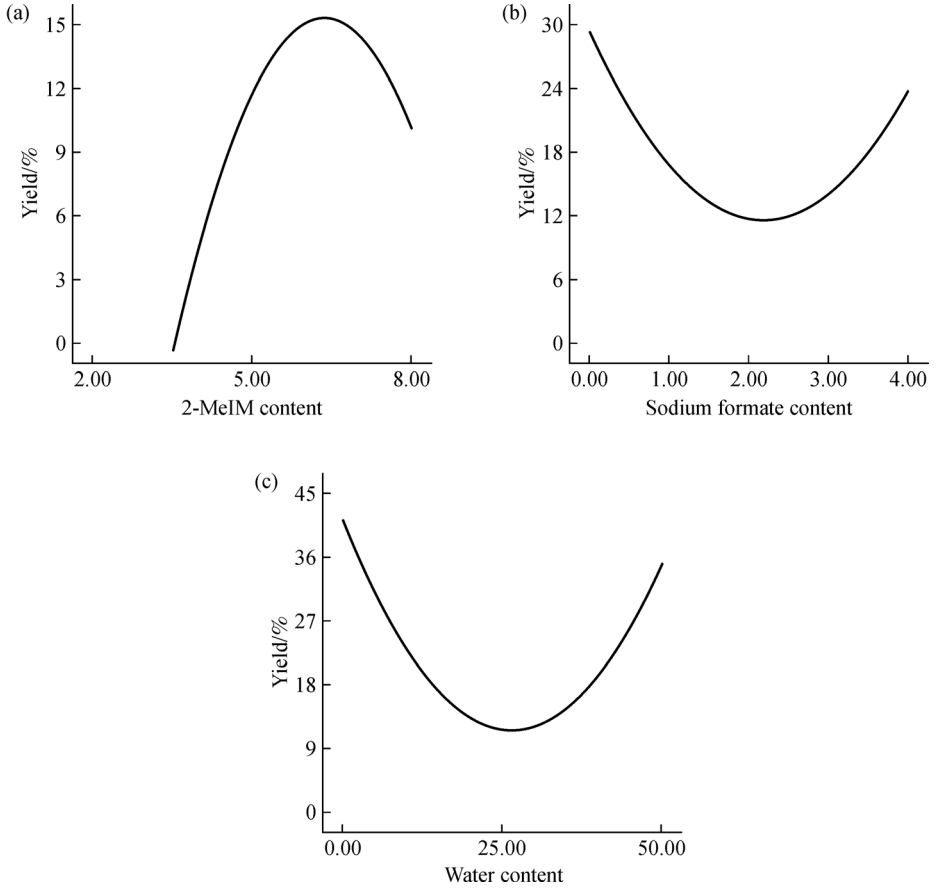

Fig. 9 One factor plots showing the effect of (a) 2-MeIM content, (b) sodium formate content, (c) water content on the yield of ZIF-8

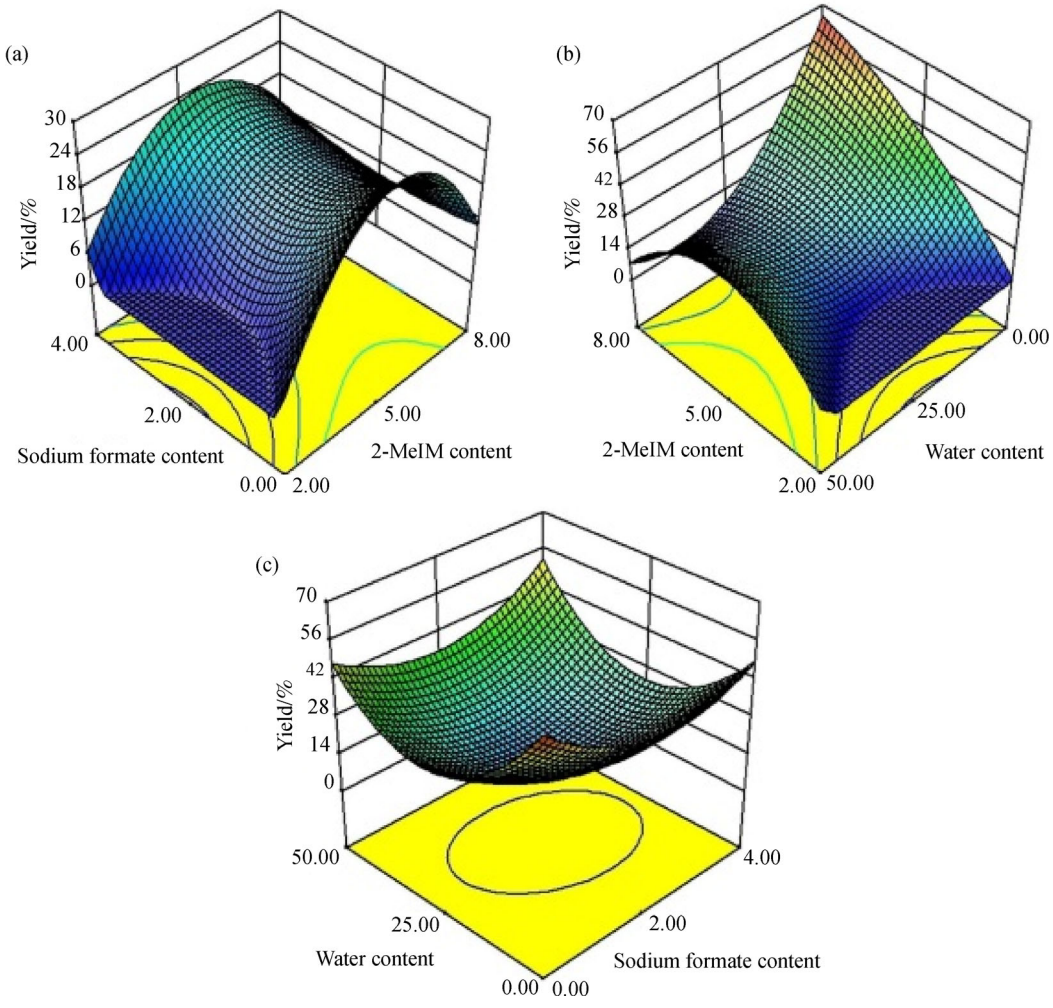

Fig. 10 Response surface plots displaying the effect of (a) 2-MeIM content and sodium formate amount, (b) 2-MeIM content and water content, and (c) sodium formate content and water content on ZIF-8 synthesis yield

In this synthetic system, sodium formate is both the modulating ligand and the deprotonating agent. The effect of the sodium formate molar content on the ZIF-8 yield is shown in Fig. 9(b). This curve shows a minimum at 2.25. At low concentrations, sodium formate works more as a deprotonating agent so it provides more imidazolium ions that assist in the growth of particles rather than producing new nuclei. This results in larger particles and a lower yield. At high concentrations, it seems that sodium formate works more as the modulating and templating agent, where it accelerates the production of new nuclei and crystals at later stages of the process. This occurs by activation of the remaining metal ions and ligands by altering the deprotonation and coordination equilibria, which enhances the ZIF-8 production yield.

The effect of the solvent on the formation process of ZIF-8 has been previous studied. The solvent can affect the process by acting as a ligand, a guest or both, and sometimes it is a structure directing agent [58]. Bustamante et al. [59] investigated the effect of the solvent on the room temperature synthesis of ZIF-8 and showed that the solvent has an important effect on the crystallization rate and the final crystal size. In addition, the solubility and reactivity of the zinc precursor have been shown to have an effect on the preparation of ZIF-8 and its morphology [47]. Here the zinc precursor and ligand were not changed, but it should be noted that their solubility may change with solvent composition. The solubility parameters for methanol, water and 2-MeIM (including their dispersion, polar, and hydrogen bond components) were used to explore the effect of water addition on the affinity between ligand and solvent. The solubility parameter distance (Ra) is used to measure the difference between the solubility parameters of two components [60]. So, in order to evaluate the solubility of 2-MeIM in methanol with and without water, the Ra values between the ligand and the various methanol-water solvents were calculated and the results are given in Tables S2 and S3. The Ra value decreased only slightly as the amount of water increased suggesting that the presence of water in the synthesis solution does not

significantly reduce the 2-MeIM solubility. In addition, because the solubility of the zinc salt in water is high, adding water to methanol does not decrease the zinc salt solubility in the mixed solvent compared to that in pure methanol. In order to experimentally investigate the solubility of the reactants with respect to the water content, each component (i.e., zinc nitrate, 2-MeIM, and sodium formate) was separately dissolved in pure methanol, and in methanol-water mixtures (containing 25 and 50 vol-% water). These solutions were then centrifuged according to the above-mentioned synthesis procedures. Interestingly, the foresaid sediment was not present in any of these centrifuged solutions. This indicates that the reduction in ZIF-8 yield that occurs with the addition of adding water is not related to the reduced solubility of the precursors. Thus the precipitated material is most probably the ZIF-8 intermediates or by-products which is supported by the XRD data (Fig. 4).

Figure 9(c) shows the effect of the water content on the yield of ZIF-8. Evidently, the crystallization rate of ZIF-8 varies in different solvents. In our experiments, the turbidity rate of the synthesis solution against time is lower in methanol-water mixtures compared to that in pure methanol which indicates that the ZIF-8 crystallization is slower in presence of water. At a water content of 25 vol-%, the ZIF-8 yield was at a minimum. These may be because lower amounts of water reduce the number of free imidazolium anions in the synthesis solution. This then hinders the produced nuclei from growing which negatively affects the ZIF-8 synthesis. The addition of further water has a different effect on ZIF-8 yield. The ability of the water to participate in hydrogen bonds makes ligand deprotonation easier, and enhances the yield by introducing more ligands for the coordination process which enhances the yield by particle growth.

3.3.2 Effect of factors on ZIF-8 particle size

The FE-SEM images of the ZIF-8 particles prepared using the first six experimental conditions in Table 3 are shown in Fig. 11. The smaller particles have rounded edges whereas the larger particles have sharper edges. Therefore, it could be inferred that the rounded particles are due to faster crystallization processes. The particle size distributions and Gaussian fits for these samples are given in Fig. 12. Clearly the ZIF-8 particle size varied greatly with synthesis conditions. The FE-SEM analysis of the ZIF-8 particles synthesized at all designed experiments are presented in Fig S1.

Figure 13 shows the effect of synthesis condition on the ZIF-8 particle size in one-factor plots. The ZIF-8 particle sizes decreased drastically as the ligand content in the synthesis medium increased (Fig. 13(a)). This is because more 2-MeIM in the reaction media leads to a higher density of nuclei which causes smaller particles. The 3D RSM plots in Figs. 14(a,b) show this decreasing trend in particle size with ligand content, except at high levels of 2-MeIM where a small increase in particle size occurs

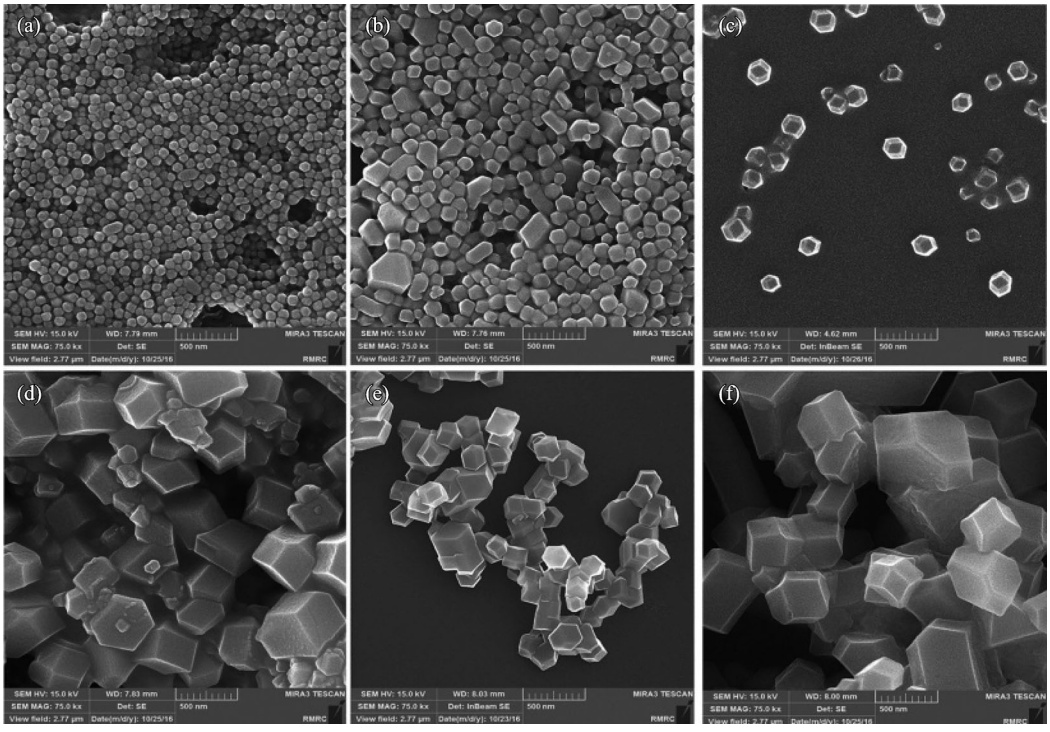

Fig. 11 (a–f) FE-SEM images of ZIF-8 particles synthesized at experimental conditions 1 to 6 (Table 3), at the same scale (500 nm)

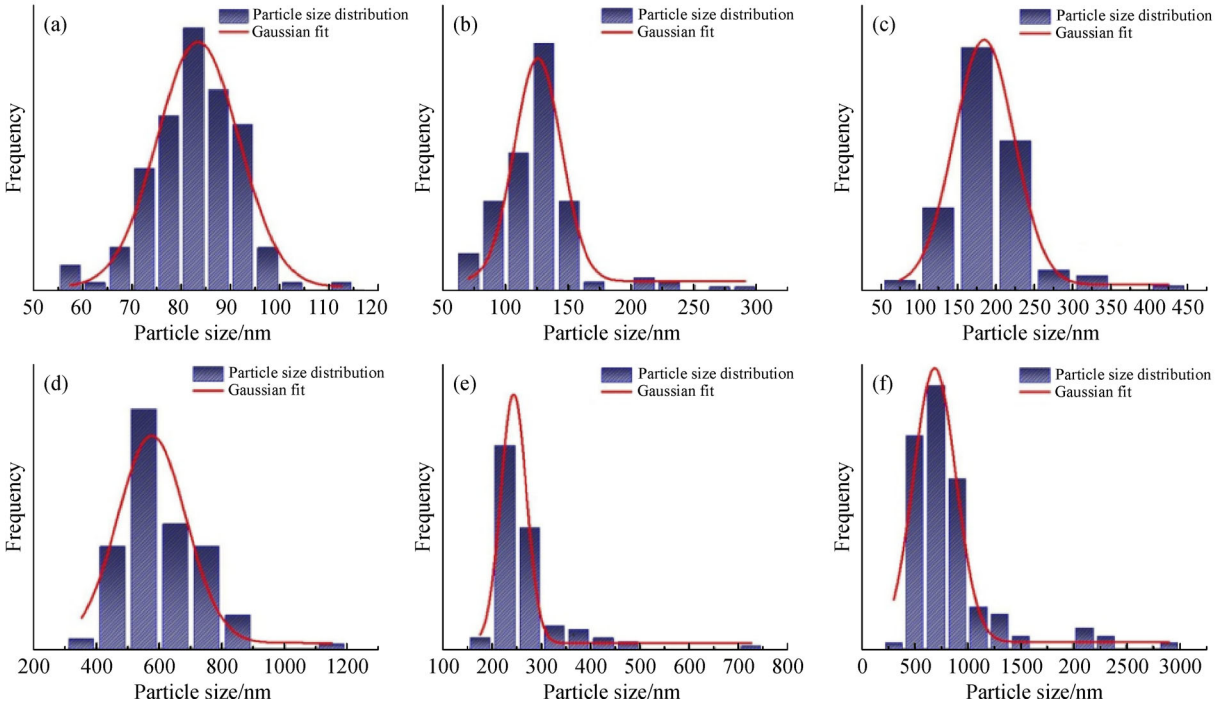

Fig. 12 (a–f) Particle size distribution and Gaussian fit of ZIF-8 particles prepared at conditions 1 to 6 (Table 3)

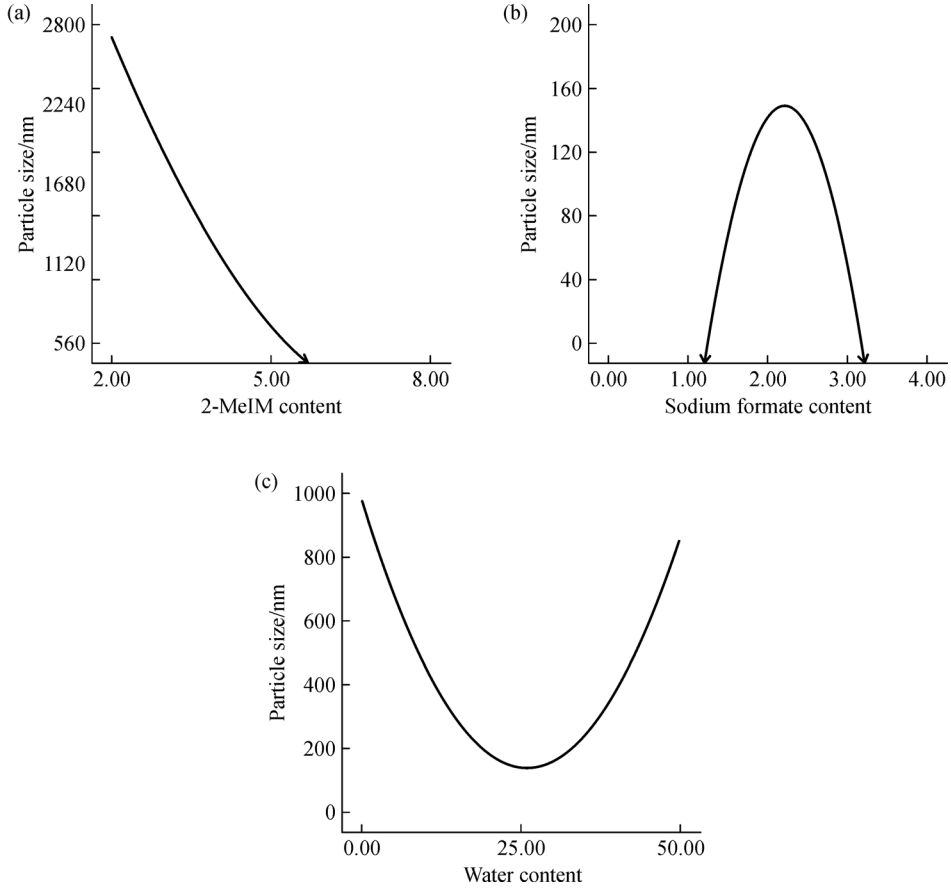

Fig. 13 One-factor plots showing the effect of (a) 2-MeIM content, (b) sodium formate content, (c) water content on the particle size of produced ZIF-8 particles

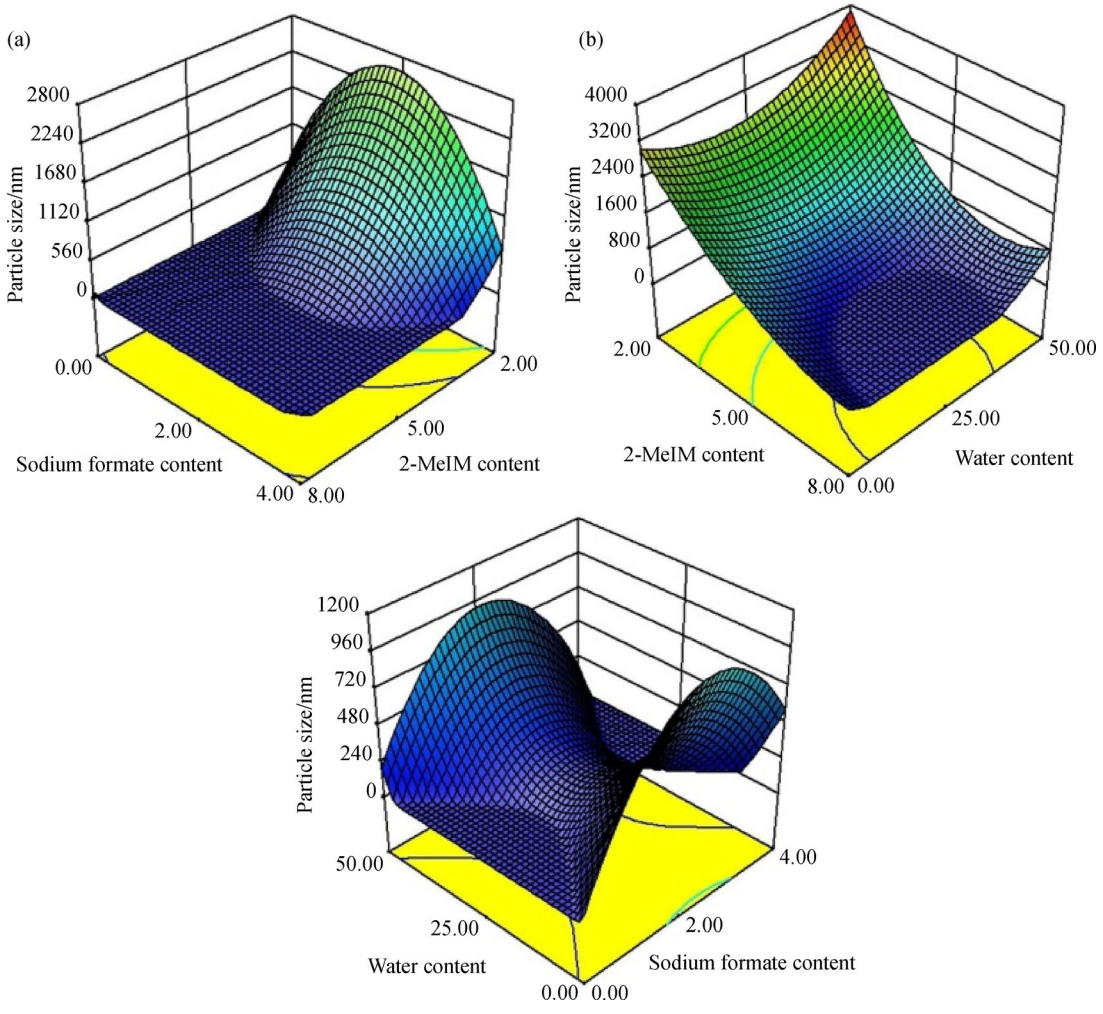

Fig. 14 3D response surface plots representative the effect of (a) 2-MeIM content and sodium formate amount, (b) 2-MeIM content and water content, and (c) sodium formate content and water content on ZIF-8 particle size

(Fig. 14(b)). When the amount of zinc is constant, by increasing in ligand content the number of nuclei reaches the maximum level, and further amount of ligand is consumed for the growth of nuclei which leads to a small rising in particle size. The curve displaying the effect of sodium formate on ZIF-8 particle size reaches a maximum at a sodium formate/zinc nitrate molar ratio of about 2.2 (Fig. 13 (b)). Since sodium formate acts as a deprotonating agent in the synthesis solution, the addition of sodium formate provides more imidazolate anions for ZIF-8 growth which leads to larger particles. However, at higher amounts of sodium formate (>2.2), the particle sizes decrease which is likely because of repulsions between the ligands and nuclei which arise from the large number of negatively charged imidazolium ions produced by the sodium formate. This phenomenon affects the growth step and makes the ZIF-8 particles smaller. The influence of water on ZIF-8 particle size is shown in Fig. 13(c). The smallest particles are obtained with 25 vol-% water. This could be due the limited number of free imidazolium ions in the presence of water which reduces the particle size by hindering the growth step. This trend differs at the higher water content (50 vol-%) because the addition of more water facilitates the deprotonation process due to the ability of water to form hydrogen bonds with ligand. The excess deprotonated ligands help the ZIF-8 to growth more. Another possibility is that a large amount of water causes the formation of zinc hydroxide which hinders the zinc cations from reacting with the ligands resulting in lower nuclei density and larger particles. The interactive effect of sodium formate and water is shown in Fig. 14(c). At a fixed water content, increasing the sodium formate concentration leads to a maximum in particle size. At lower concentrations, increasing the sodium formate content results in more deprotonation of the ligands and consequently larger particle sizes. At the highest levels of sodium formate, the high amount of deprotonation creates more nuclei and also creates repulsions between the ligand

and nuclei which cause the formation of smaller particles. The minimum for 25% water was explained previously in the discussion of Fig. 13(c).

3.3.3 Optimization of ZIF-8 synthesis yield

One of the most useful applications of RSM is to optimize processes in terms of the selected parameters. Here, two responses, ZIF-8 yield and mean particle size, were studied. Since the optimum value of particle size depends on the desired application for those particles, particle size was excluded and the optimization was carried out only to maximize the ZIF-8 synthesis yield. Based on the RSM results an optimal ZIF-8 yield of 67.13% can be achieved with a 2-MeIM/metal salt ratio of 6.32, a sodium formate/metal salt ratio of 0.09, and a water content of 0.54 vol-%. Under these conditions, the ZIF-8 mean particle size is predicted to be about 105 nm.

3.4 Carbon monoxide adsorption on ZIF-8 particles

There have been few studies on the relationship between adsorption capacity and MOF particle size [61]. So, ZIF-8 particles with three different particle sizes (100, 500 and 1000 nm) were used for the static adsorption of CO and the results are shown in Fig. 15. The synthesis conditions used to prepare these samples are given in Table S6 (cf. ESM). The highest CO adsorption (0.67 mmol/g at 9.15 bar) was obtained with the mid-size ZIF-8 particles which is about 5% and 33% higher than those obtained with the large (1000 nm) and ultrafine (100 nm) ZIF-8 particles at the same pressure, respectively.

The most crucial aspect of gas adsorption on the MOFs is the activation of the pores by the removal of the solvent molecules from the surface pore apertures [62]. This never completely happens and so blocked surface pores are a major problem for gas adsorption on the MOFs. This problem becomes more pronounced at smaller particle sizes [61]. By decreasing the particle size, the exposure of defected surface pores of each ZIF-8 particle to the CO gas molecules becomes higher which causes the reduction of CO adsorption capacity in fine ZIF-8 nanoparticles (about 100 nm). On the other hand, an increase in the particle size results in smaller specific surface areas which also adversely affects the adsorption process. Therefore, as confirmed experimentally (Fig. 15), the optimum ZIF-8 particle size for adsorption of CO molecules is the mid-sized particles. It should be noted that there is an unstable region at low pressures (0 – 4 bar) where the adsorption capacity trends are different. This behavior could be due to the swinging of the imidazolate linker and gate opening effect of ZIF-8 particles occurs at higher pressures [63].

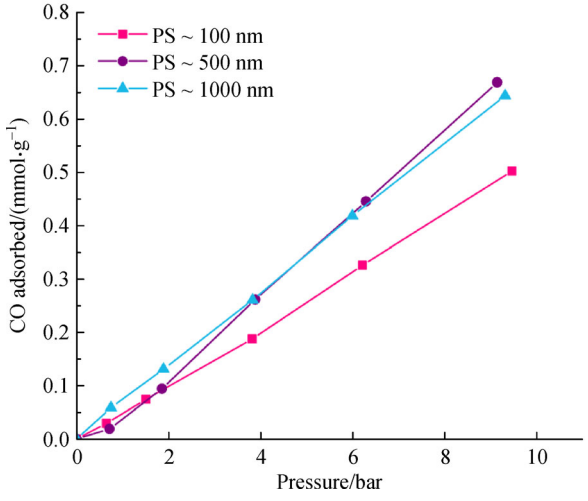

Fig. 15 CO adsorption capacity of ZIF-8 samples with different particle sizes (PS)

4 Conclusions

ZIF-8 particles were synthesized at room temperature in mixed solvents in order to study the effect of the synthesis parameters on yield and particle size. The prepared particles were characterized using various techniques. N_2 adsorption-desorption isotherm confirmed the microporosity of the ZIF-8 particles and TGA verified the high thermal stability of the ZIF-8 structure up to 400°C. The sizes of the prepared particles were measured using FE-SEM. Response surface methodology was used to explore the effect of the synthesis parameters on the ZIF-8 yield and particle size. A cubic form model best described (p-value $< < 0.05$) both the ZIF-8 yield and mean particle size at different synthesis conditions. The ligand content had a large effect on both the ZIF-8 preparation yield and particle size. Almost all synthesis conditions produced ZIF-8 particles with relatively narrow size distributions. ZIF-8 particles with a wide range of sizes (83 nm to 3.8 μm) were easily prepared by changing the synthesis condition. Results revealed that ZIF-8 particle size could be controlled by solvent composition. The size variations were the result of the different hydrogen donation abilities of methanol and water, the formation of zinc hydroxide, and the difference in ligand availability in the presence of water. The remarkable effect of solvent composition on the ZIF-8 particle size shows that this mixed solvent system is a versatile technique for the manipulation of ZIF-8 particle size by controlling the crystallization rate. These ZIF-8 samples with different particle sizes were used for CO adsorption and the 500-nm particles were the optimal size for the adsorption process.

Electronic Supplementary Material Supplementary material is available in the online version of this article at https://doi.org/10.1007/s11705–018–1770–3 and is accessible for authorized users.

References

1. Furukawa H, Cordova K E, O'Keeffe M, Yaghi O M. The chemistry and applications of metal-organic frameworks. Science, 2013, 341 (6149): 1–12
2. Farrusseng D. Metal-Organic Frameworks: Applications from Catalysis to Gas Storage. Hoboken:Weinheim Wiley-VCH, 2011
3. Cheong V F, Moh P Y. Recent advancement in metal–organic framework: Synthesis, activation, functionalisation, and bulk production. Materials Science and Technology, 2018, 34(9): 1025–1045
4. Yan D, Lloyd G O, Delori A, Jones W, Duan X. Tuning fluorescent molecules by inclusion in a metal-organic framework: An experimental and computational study. ChemPlusChem, 2012, 77(12): 1112–1118
5. Kurmoo M. Magnetic metal-organic frameworks. Chemical Society Reviews, 2009, 38(5): 1353–1379
6. Zhang C F, Qiu L G, Ke F, Zhu Y J, Yuan Y P, Xu G S, Jiang X. A novel magnetic recyclable photocatalyst based on a core-shell metal-organic framework Fe_3O_4@MIL-100(Fe) for the decolorization of methylene blue dye. Journal of Materials Chemistry. A, Materials for Energy and Sustainability, 2013, 1(45): 14329–14334
7. Wu Y N, Zhou M, Li S, Li Z, Li J, Wu B, Li G, Li F, Guan X. Magnetic metal-organic frameworks: γ-Fe_2O_3@MOFs via confined *in situ* pyrolysis method for drug delivery. Small, 2014, 10(14): 2737–2962
8. Lin K A, Chang H A, Hsu C J. Iron-based metal organic framework, MIL-88A, as a heterogeneous persulfate catalyst for decolorization of Rhodamine B in water. RSC Advances, 2015, 5(41): 32520–32530
9. Kayal S, Sun B, Chakraborty A. Study of metal-organic framework MIL-101(Cr) for natural gas (methane) storage and compare with other MOFs (metal-organic frameworks). Energy, 2015, 91: 772–781
10. Ren J, Musyoka N M, Langmi H W, North B C, Mathe M, Kang X, Liao S. Hydrogen storage in Zr-fumarate MOF. International Journal of Hydrogen Energy, 2015, 40(33): 10542–10546
11. Jusoh N, Yeong Y F, Cheong W L, Lau K K, Shariff A M. Facile fabrication of mixed matrix membranes containing 6FDA-durene polyimide and ZIF-8 nanofillers for CO_2 capture. Journal of Industrial and Engineering Chemistry, 2016, 44: 164–173
12. Erucar I, Keskin S. Computational assessment of MOF membranes for CH_4/H_2 separations. Journal of Membrane Science, 2016, 514: 313–321
13. Adatoz E, Avci A K, Keskin S. Opportunities and challenges of MOF-based membranes in gas separations. Separation and Purification Technology, 2015, 152: 207–237
14. Melgar V M A, Ahn H, Kim J, Othman M R. Highly selective micro-porous ZIF-8 membranes prepared by rapid electrospray deposition. Journal of Industrial and Engineering Chemistry, 2015, 21: 575–579
15. Sarfraz M, Ba-Shammakh M. Synergistic effect of incorporating ZIF-302 and graphene oxide to polysulfone to develop highly selective mixed-matrix membranes for carbon dioxide separation from wet post-combustion flue gases. Journal of Industrial and Engineering Chemistry, 2016, 36: 154–162
16. Wang Y, Li C, Meng F, Lv S, Guo J, Liu X, Wang C, Ma Z. $CuAlCl_4$ doped MIL-101 as a high capacity CO adsorbent with selectivity over N_2. Frontiers of Chemical Science and Engineering, 2014, 8(3): 340–345
17. Dang G H, Lam H Q, Nguyen A T, Le D T, Truong T, Phan N T S. Synthesis of indolizines through aldehyde-amine-alkyne couplings using metal-organic framework Cu-MOF-74 as an efficient heterogeneous catalyst. Journal of Catalysis, 2016, 337: 167–176
18. Liu J, Chen L, Cui H, Zhang J, Zhang L, Su C Y. Applications of metal–organic frameworks in heterogeneous supramolecular catalysis. Chemical Society Reviews, 2014, 43(16): 6011–6061
19. Hu Y, Zheng S, Zhang F. Fabrication of MIL-100(Fe)@SiO_2@-Fe_3O_4 core-shell microspheres as a magnetically recyclable solid acidic catalyst for the acetalization of benzaldehyde and glycol. Frontiers of Chemical Science and Engineering, 2016, 10(4): 534–541
20. Li Q L, Wang J P, Liu W C, Zhuang X Y, Liu J Q, Fan G L, Li B H, Lin W N, Man J H. A new (4,8)-connected topological MOF as potential drug delivery. Inorganic Chemistry Communications, 2015, 55: 8–10
21. Singco B, Liu L, Chen Y, Shih Y H, Huang H Y, Lin C H. Approaches to drug delivery: Confinement of aspirin in MIL-100 (Fe) and aspirin in the *de novo* synthesis of metal-organic frameworks. Microporous and Mesoporous Materials, 2016, 223: 254–260
22. Barea E, Montoro C, Navarro J A R. Toxic gas removal—metal-organic frameworks for the capture and degradation of toxic gases and vapours. Chemical Society Reviews, 2014, 43(16): 5419–5430
23. Hosseini M S, Zeinali S, Sheikhi M H. Fabrication of capacitive sensor based on Cu-BTC (MOF-199) nanoporous film for detection of ethanol and methanol vapors. Sensors and Actuators. B, Chemical, 2016, 230: 9–16
24. Li W, Wu X, Han N, Chen J, Qian X, Deng Y, Tang W, Chen Y. MOF-derived hierarchical hollow ZnO nanocages with enhanced low-concentration VOCs gas-sensing performance. Sensors and Actuators. B, Chemical, 2016, 225: 158–166
25. Wang K M, Du L, Ma Y L, Zhao Q H. Selective sensing of 2,4,6-trinitrophenol and detection of the ultralow temperature based on a dual-functional MOF as a luminescent sensor. Inorganic Chemistry Communications, 2016, 68: 45–49
26. Wang L, Han Y, Feng X, Zhou J, Qi P, Wang B. Metal-organic frameworks for energy storage: Batteries and supercapacitors. Coordination Chemistry Reviews, 2016, 307: 361–381
27. Zhang Y, Niu Y B, Liu T, Li Y T, Wang M Q, Hou J, Xu M. A nickel-based metal-organic framework: A novel optimized anode material for Li-ion batteries. Materials Letters, 2015, 161: 712–715
28. Park K S, Ni Z, Côté A P, Choi J Y, Huang R, Uribe-Romo F J, Chae H K, O'Keeffe M, Yaghi O M. Exceptional chemical and thermal stability of zeolitic imidazolate frameworks. Proceedings of the National Academy of Sciences of the United States of America, 2006, 103(27): 10186–10191
29. Tu M, Wiktor C, Rosler C, Fischer R A. Rapid room temperature syntheses of zeoliticimidazolate framework (ZIF) nanocrystals. Chemical Communications, 2014, 50: 13258–13260
30. Munn A S, Dunne P W, Tang S V Y, Lester E H. Large-scale continuous hydrothermal production and activation of ZIF-8.

Chemical Communications, 2015, 51: 12811–12814
31. Cravillon J, Schröder C A, Bux H, Rothkirch A, Caro J, Wiebcke M. Formate modulated solvothermal synthesis of ZIF-8 investigated using time-resolved *in situ* X-ray diffraction and scanning electron microscopy. CrystEngComm, 2012, 14(2): 492–498
32. Cho H Y, Kim J, Kim S N, Ahn W S. High yield 1-L scale synthesis of ZIF-8 via a sonochemical route. Microporous and Mesoporous Materials, 2013, 169: 180–184
33. Friščić T, Halasz I, Beldon P J, Belenguer A M, Adams F, Kimber S A J, Honkimäki V, Dinnebier R E. Real-time and *in situ* monitoring of mechanochemical milling reactions. Nature Chemistry, 2013, 5: 66–73
34. Joaristi A M, Alcañiz J J, Crespo P S, Kapteijn F, Gascon J. Electrochemical synthesis of some archetypical Zn^{2+}, Cu^{2+}, and Al^{3+} metal organic frameworks. Crystal Growth & Design, 2012, 12(7): 3489–3498
35. Shi Q, Chen Z, Song Z, Li J, Dong J. Synthesis of ZIF-8 and ZIF-67 by steam-assisted conversion and an investigation of their tribological behaviors. Angewandte Chemie International Edition, 2010, 50(3): 672–675
36. Liu W, Zhao Y, Zeng C, Wang C, Serra C A, Zhang L. Microfluidic preparation of yolk/shell ZIF-8/alginate hybrid microcapsules from Pickering emulsion. Chemical Engineering Journal, 2017, 307: 408–417
37. Butova V V, Budnik A P, Bulanova E A, Soldatov A V. New microwave-assisted synthesis of ZIF-8. Mendeleev Communications, 2016, 26(1): 43–44
38. Schejn A, Balan L, Falk V, Aranda L, Medjahdi G, Schneider R. Controlling ZIF-8 nano- and microcrystal formation and reactivity through zinc salt variations. CrystEngComm, 2014, 16(21): 4493–4500
39. Zhou J, Yu X, Fan X, Wang X, Li H, Zhang Y, Li W, Zheng J, Wang B, Li X. The impact of the particle size of a metal-organic framework for sulfur storage in Li–S batteries. Journal of Materials Chemistry. A, Materials for Energy and Sustainability, 2015, 3(16): 8272–8275
40. Linder-Patton O M, Bloch W M, Coghlan C J, Sumida K, Kitagawa S, Furukawa S, Doonana C J, Sumby C J. Particle size effects in the kinetic trapping of a structurally-locked form of a flexible MOF CrystEngComm, 2016, 18(22): 4172–4179
41. Nordin N A H M, Ismail A F, Mustafa A, Murali R S, Matsuura T. The impact of ZIF-8 particle size and heat treatment on CO_2/CH_4 separation using asymmetric mixed matrix membrane. RSC Advances, 2014, 4(94): 52530–52541
42. Ban Y, Li Y, Liu X, Peng Y, Yang W. Solvothermal synthesis of mixed-ligand metal-organic framework ZIF-78 with controllable size and morphology. Microporous and Mesoporous Materials, 2013, 173: 29–36
43. Cravillon J, Nayuk R, Springer S, Feldhoff A, Huber K, Wiebcke M. Controlling zeolitic imidazolate framework nano- and microcrystal formation: insight into crystal growth by time-resolved *in situ* static light scattering. Chemistry of Materials, 2011, 23(8): 2130–2141
44. Peralta D, Chaplais G, Simon-Masseron A, Barthelet K, Pirngruber G D. Synthesis and adsorption properties of ZIF-76 isomorphs. Microporous and Mesoporous Materials, 2012, 153: 1–7
45. Polyzoidis A, Altenburg T, Schwarzer M, Loebbecke S, Kaskel S. Continuous microreactor synthesis of ZIF-8 with high space-time-yield and tunable particle size. Chemical Engineering Journal, 2016, 283: 971–977
46. Jian M, Liu B, Liu R, Qu J, Wang H, Zhang X. Water-based synthesis of zeolitic imidazolate framework-8 with high morphology level at room temperature. RSC Advances, 2015, 5(60): 48433–48441
47. Chi W S, Hwang S, Lee S J, Park S, Bae Y S, Ryu D Y, Kim J H, Kim J. Mixed matrix membranes consisting of SEBS block copolymers and size-controlled ZIF-8 nanoparticles for CO_2 capture. Journal of Membrane Science, 2015, 495: 479–488
48. Cravillon J, Münzer S, Lohmeier S J, Feldhoff A, Huber K, Wiebcke M. Rapid room-temperature synthesis and characterization of nanocrystals of a prototypical zeolitic imidazolate framework. Chemistry of Materials, 2009, 21(8): 1410–1412
49. Zhang C, Lively R P, Zhang K, Johnson J R, Karvan O, Koros W J. Unexpected molecular sieving properties of zeolitic imidazolate framework-8. Journal of Physical Chemistry Letters, 2012, 3(16): 2130–2134
50. Bezerra M A, Erthal R, Eliane S, Oliveira P, Silveira L, Luciane V, Escaleira A. Response surface methodology (RSM) as a tool for optimization in analytical chemistry. Talanta, 2008, 76(5): 965–977
51. Talib N A, Salam F, Yusof N A, Ahmad S A A, Sulaiman Y. Optimization of peak current of poly(3,4-ethylenedioxythiophene)/multi-walled carbon nanotube using response surface methodology/central composite design. RSC Advances, 2017, 7(18): 11101–11110
52. Nordin N A H M, Ismail A F, Mustafa A, Goh P S, Rana D, Matsuura T. Aqueous room temperature synthesis of zeolitic imidazole framework 8 (ZIF-8) with various concentrations of triethylamine. RSC Advances, 2014, 4(63): 33292–33300
53. James J B, Lin Y S. Kinetics of ZIF-8 thermal decomposition in inert, oxidizing and reducing environments. Journal of Physical Chemistry C, 2016, 120(26): 14015–14026
54. Lai L S, Yeong Y F, Lau K K, Azmi M S. Zeolite imidazole frameworks membranes for CO_2/CH_4 separation from natural gas: A review. Journal of Applied Sciences (Faisalabad), 2014, 14(11): 1161–1167
55. Beh J J, Lim J K, Ng E P, Ooi B S. Synthesis and size control of zeolitic imidazolate framework-8 (ZIF-8): From the perspective of reaction kinetics and thermodynamics of nucleation. Materials Chemistry and Physics, 2018, 216: 393–401
56. Tanaka S, Kida K, Okita M, Ito Y, Miyake Y. Size-controlled synthesis of zeolitic imidazolate framework-8 (ZIF-8) crystals in an aqueous system at room temperature. Chemistry Letters, 2012, 41: 1337–1339
57. Kida K, Okita M, Fujita K, Tanaka S, Miyake Y. Formation of high crystalline ZIF-8 in an aqueous solution. CrystEngComm, 2013, 15 (9): 1794–1801
58. Li C P, Du M. Role of solvents in coordination supramolecular systems. Chemical Communications, 2011, 47(21): 5958–5972
59. Bustamante E L, Fernández J L, Zamaro J M. Influence of the solvent in the synthesis of zeolitic imidazolate framework-8 (ZIF-8) nanocrystals at room temperature. Journal of Colloid and Interface Science, 2014, 424: 37–43
60. Hadi A, Karimi-Sabet J, Moosavian S M A, Ghorbanian S.

Optimization of graphene production by exfoliation of graphite in supercritical ethanol: A response surface methodology approach. Journal of Supercritical Fluids, 2016, 107: 92–105

61. Fan X, Zhou J, Wang T, Zheng J, Li X. Opposite particle size effects on the adsorption kinetics of ZIF-8 for gaseous and solution adsorbates. RSC Advances, 2015, 5: 58595–58599
62. Mondloch J E, Karagiaridi O, Farha O K, Hupp J T. Activation of metal-organic framework materials. CrystEngComm, 2013, 15: 9258–9264
63. Casco M E, Cheng Y Q, Daemen L L, Fairen-Jimenez D, Ramos-Fernández E V, Silvestre-Albero A J R C J. Gate-opening effect in ZIF-8: The first experimental proof using inelastic neutron scattering. Chemical Communications (Cambridge), 2016, 52: 3639–3642